JOURNAL OF SOLID STATE CHEMISTRY 62, 281–289 (1986)

The Oxygen Defect Perovskite $Sr_2Mn_2O_5$: HREM Study

VINCENT CAIGNAERT, MARYVONNE HERVIEU, NINH NGUYEN, AND BERNARD RAVEAU

Laboratoire de Cristallographie, Chimie et Physique des Solides, L.A. 251, ISMRa-Université, 14032 Caen Cedex, France

Received February 1, 1985; in revised form June 12, 1985

$Sr_2Mn_2O_5$ was investigated by high-resolution electron microscopy (HREM). Numerous crystals are characterized by a regular contrast, corresponding to the tunnel structure $Sr_2Mn_2O_5$ which can be described as an ordered oxygen-defect perovskite ($a = a_P\sqrt{2}$, $b = 2a_P\sqrt{2}$, and $c \simeq a_P$). Several types of defects were observed and interpreted in terms of different orderings of oxygen vacancies: $Sr_2Mn_2O_5$-type domains with antiphase boundaries (APB), $Sr_2Mn_2O_5$-type domains with perovskite domains, new ordered domains ($a \simeq a_P\sqrt{2}$ and $b \simeq 4a_P\sqrt{2}$), and stacking faults.

Introduction

It is well known that electrocatalytic and electrode properties of the oxygen-defects perovskites ABO_{3-x} have their origin in the nature of the B cations which can take simultaneously several oxidation states and several coordinations as shown, for example, for copper oxides (*1*). In this respect, manganese perovskites $AMnO_{3-x}$ (*2–10*) seem to offer large possibilities due to the ability of manganese to take the two oxidation states, III and IV, and to have both octahedral and pyramidal coordinations. Besides the calcium perovskites whose structures have been recently studied (*2–7*), several phases have been isolated in the case of strontium manganese oxides (*8, 9*). However, these latter oxides, which exhibit complex arrangements of the oxygen vacancies have not been studied by electron microscopy so that little is known about their defect structure. In a recent paper (*10*), it was shown that $Sr_2Mn_2O_5$ could be synthesized with the $Ca_2Mn_2O_5$ (*7*) structure. The present work deals with the high-resolution electron microscopy, HREM, study of the defects which appear in the crystals corresponding to samples with this nominal composition.

Experimental

The synthesis of $Sr_2Mn_2O_5$ has already been described (*10*). It consists in heating adequate mixtures of $SrCO_3$ and Mn_3O_4 first in air at 1150 and 1450°C successively, then in evacuated ampoule at 500°C in the presence of zirconium. The oxygen amount was determined by chemical analysis as previously described (*10*): only the samples corresponding to the composition $Sr_2Mn_2O_5$ were examined by electron microscopy.

High-resolution electron microscopic observations were made at 120 kV with a JEM 120 CX electron microscope equipped with

0022-4596/86 $3.00

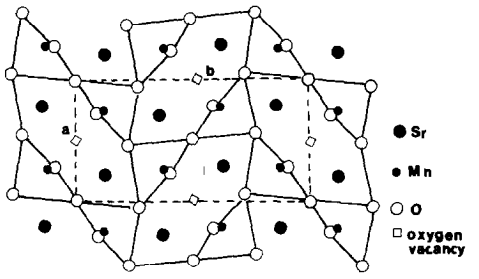

FIG. 1. Projection along [001] of the oxygen-defect perovskite $Sr_2Mn_2O_5$.

a top-entry double tilt (±10°) goniometer specimen holder and an objective lens with spherical (C_S) aberration coefficient of 0.7 mm. The samples were crushed in an agate mortar and then mounted on a holey carbon film. Thin fragments were oriented, mainly with [001] exactly parallel to the electron beam, as indicated by the selected-area electron diffraction patterns. Image astigmatism was corrected by observing the granularity of the support carbon films and areas of thin oriented crystals, protruding over holes, were chosen for imaging. Multislice N-beam calculations were carried out with programs supplied by Skarnulis (*13*). Through-focus series were calculated for various thicknesses of the crystals.

Structure of $Sr_2Mn_2O_5$. The structure of $Sr_2Mn_2O_5$ (*10*) is characterized by an orthorhombic cell with a = 5.523(1) Å, b = 10.761(5) Å, and c = 3.811(1) Å. The host lattice "Mn_2O_5" (Fig. 1) is built up from corner-sharing MnO_5 pyramids forming pseudo-hexagonal tunnels running along ⟨001⟩ and perovskite tunnels running

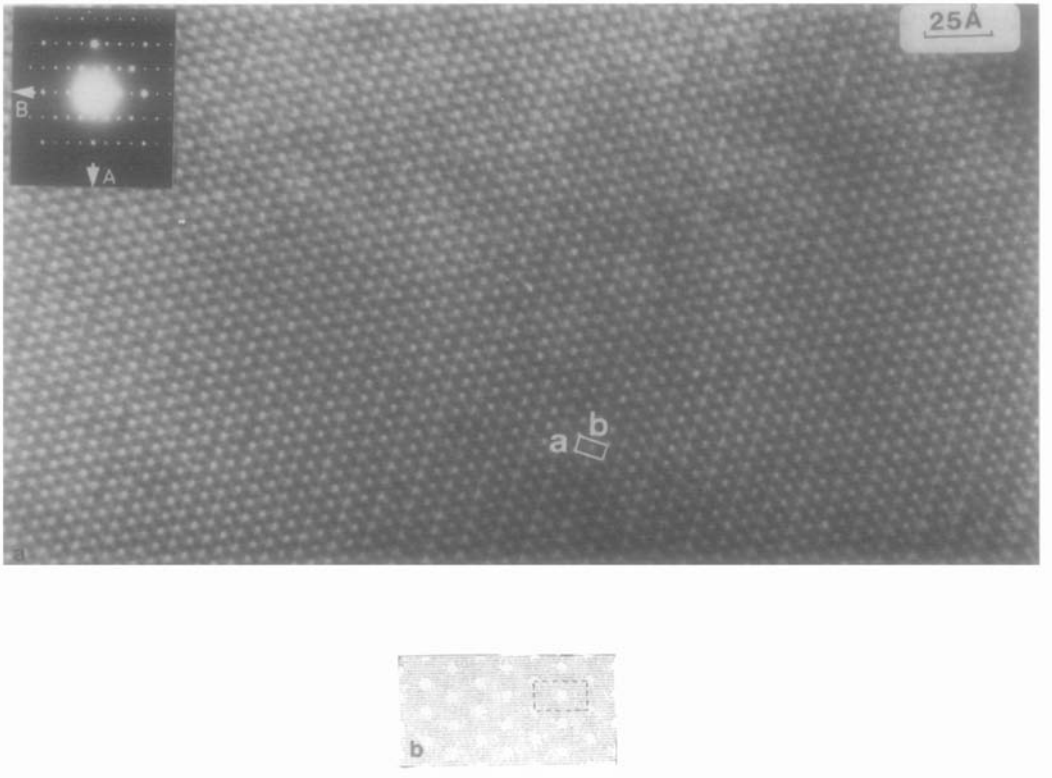

FIG. 2. (a) Lattice image of a crystal of $Sr_2Mn_2O_5$ obtained from [001] zone diffraction pattern. (b) Calculated image (4 × 4): thickness = 38 Å, defocus setting F = −600 Å. (The drawn cell is translated from $a/2$ with regard to the crystallographic origin.)

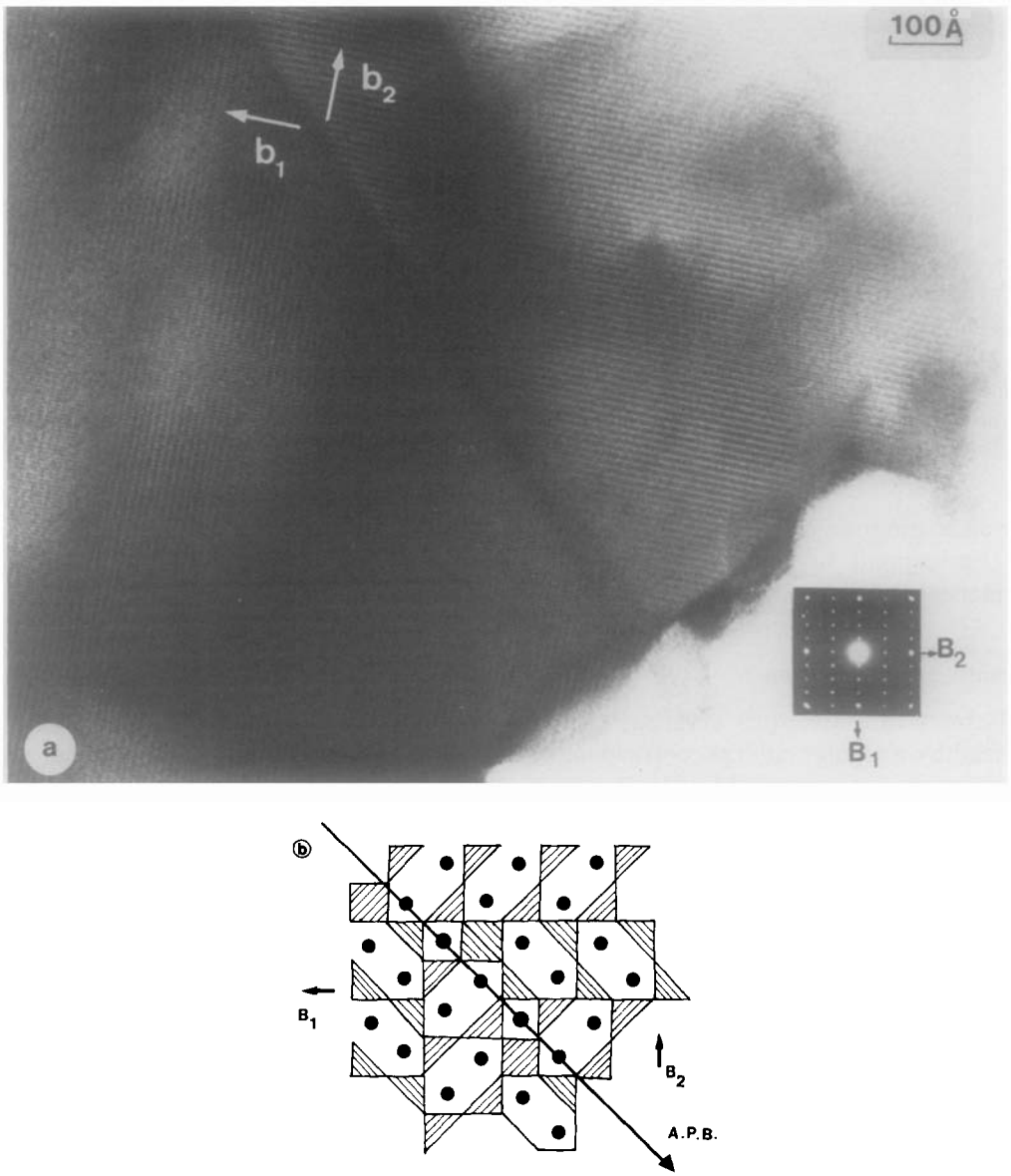

FIG. 3. (a) Micrograph, as a projection along [001], of two adjacent microdomains exhibiting a $Sr_2Mn_2O_5$-type structure. They are characterized by an angle of 90° between the two *b* axis: (b) Idealized drawing of the two orientated domains and their junction.

along ⟨110⟩ and ⟨1$\bar{1}$0⟩. The occurence of oxygen-defect ordering results in a tilting of the MnO_5 pyramids around the *c* axis; the angles between the oxygen of two neighboring pyramids is close to 74° (instead of 90° in the ideal structure). A large number of crystals exhibit images of this tunnel structure as shown from Fig. 2a taken along the [001] zone. In this image it was concluded from the calculated images (Fig. 2b) that

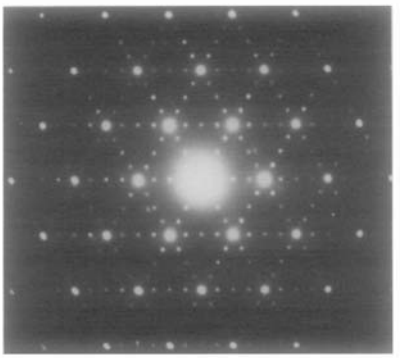

FIG. 4. Electron diffraction pattern showing the superstructure ($a \simeq 2a_p \sqrt{2}$) along the three directions $\langle 110 \rangle_P$.

the alternate rows of bright dots, spaced 5.5 Å, correspond to the pseudo-hexagonal tunnels (*10*).

Results and Discussion

Besides the numerous crystals, characterized by a regular contrast corresponding to the tunnel structure of $Sr_2Mn_2O_5$, many crystals were found to exhibit defects. This work is focused on the main types of defects which were observed and the possible corresponding arrangement of the oxygen vacancies.

$Sr_2Mn_2O_5$-Type Domains and Antiphase Boundaries

The observations along $\vec{c}$ show that many crystals exhibit twinned domains exhibiting the $Sr_2Mn_2O_5$ structure. They are characterized (Fig. 3) by an angle of 90° between the two "*b*" directions and an orientation domain boundary parallel to (120), i.e., to $(100)_P$. The junction between two adjacent domains is easily explained by a slight local variation of stoichiometry (Fig. 3b) involving the presence of MnO_6 octahedra at the domain boundary. It is evident that such a variation of oxygen content could be too small to be detected by chemical analysis. This tendancy to form domains comes from the fact that the ordering of the oxygen vacancies in the original cubic perovskite cell (a_P), leading to the superstructure $a \simeq a_P \sqrt{2}$ and $b \simeq 2\sqrt{2}a_P$, can take place along three equivalent directions in the perovskite matrix. Indeed many crystals exhibit an electron diffraction pattern of the (041) plane, i.e. of $(111)_P$, characterized by the expected superstructures along the three directions $\langle 110 \rangle_P$ with respect to the cubic perovskite subcell (Fig. 4). It must be noticed that, when this type of pattern was observed, good images could not be obtained because the crystals were too thick.

A second type of boundary (APB) is often observed in the crystals, it corresponds to a relative translation of $\vec{b}/2$ of the adjacent domains (Fig. 5a). Again, the junction between two domains (Fig. 5b) can easily be explained by the presence of octahedra involving a slight variation of local stoichiometry; this type of boundary, parallel to $\vec{c}$, is often parallel to $\vec{b}$ or $\langle 110 \rangle$ but may also wander in the bulk.

The formation of such domains appears as a general feature due to the ordering of vacancies in the cubic perovskite matrix: ordered domains, with different orientations, have also been observed in $CaMnO_{2.8}$ (*3–5*).

$Sr_2Mn_2O_5$-Type Domains and "Pseudo-cubic" Perovskite Domains

Crystals in which domains exhibit a different crystallographic cell were also observed. Figure 6 shows an example of micrograph which was obtained by observation along *c*; this type of crystal exhibits two domains: the first one (I) exhibits the $Sr_2Mn_2O_5$ structure ($a \simeq a_P \sqrt{2}$ and $b \simeq 2a_P \sqrt{2}$), the other (II) corresponds to a perovskite cell without any superstructure ($a \simeq a_P$). The boundary between the two domains is approximatively planar and corresponds to the $(120)_P$ plane of the perovskite cell. It must also be noted that

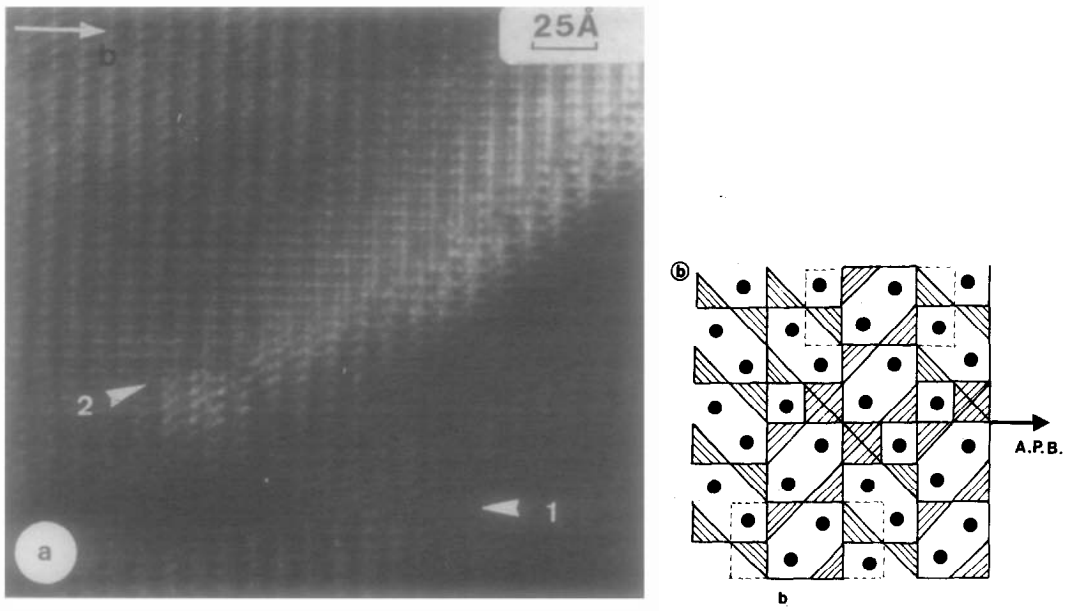

FIG. 5. Micrograph of $Sr_2Mn_2O_5$, along [001], showing the existence of antiphase boundaries corresponding to a translation of $b/2$ of the adjacent domains (white arrows). (b) As an example, idealized drawing of an antiphase boundary, parallel to b with a translation of $b/2$.

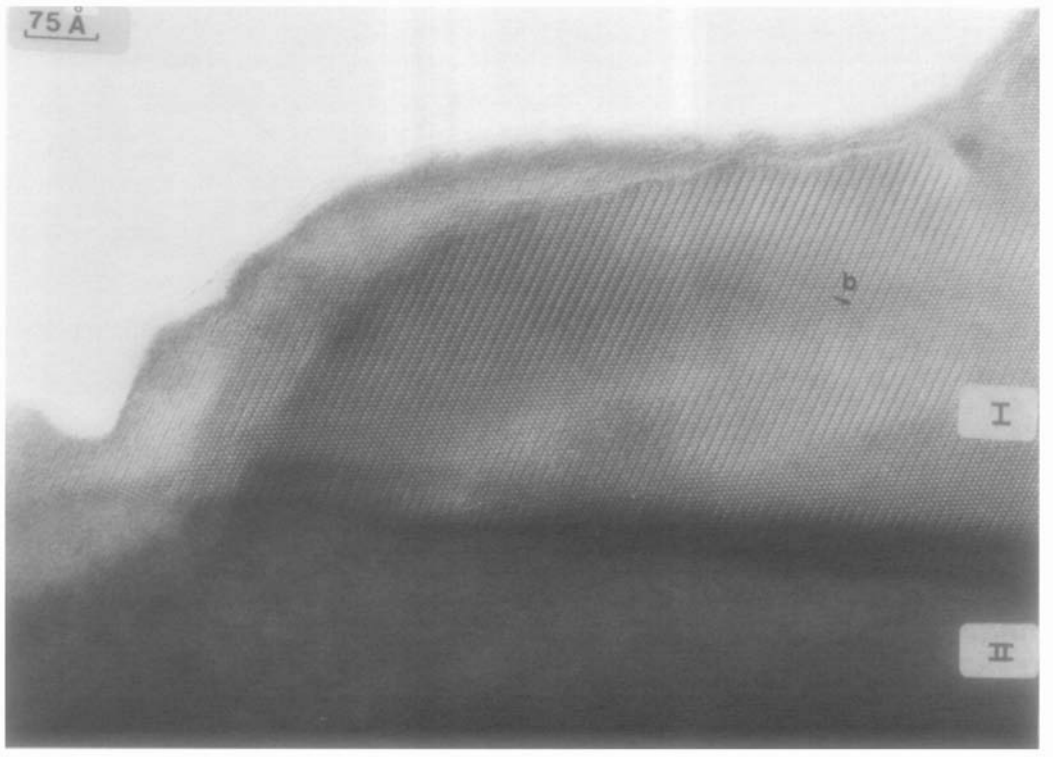

FIG. 6. Micrograph showing adjacent microdomains (projection along [001]): (I) with the $Sr_2Mn_2O_5$-type structure and (II) without any superstructure. The corresponding electron diffraction pattern does not exhibit extra spots.

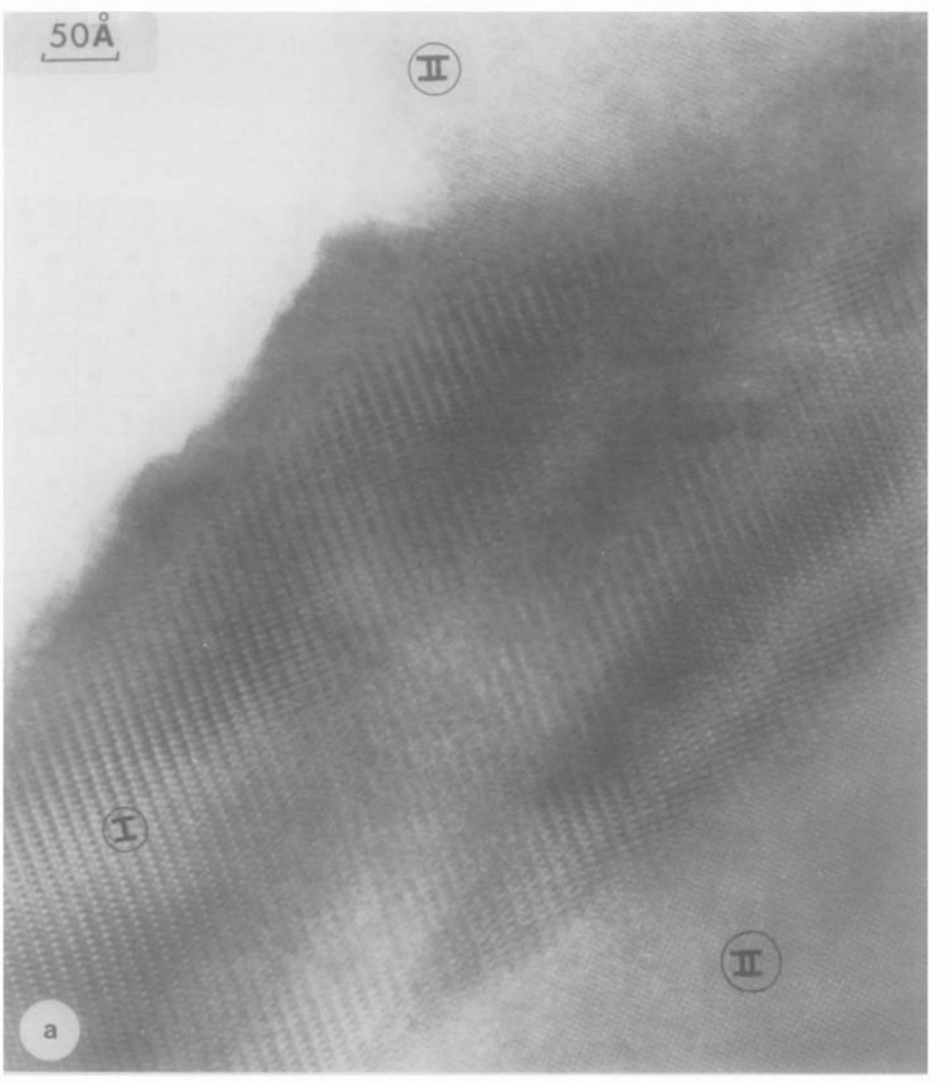

FIG. 7. Image of wandering boundaries between microdomains of type (I) and (II). (b) Idealized drawing of the superposition of two $Sr_2Mn_2O_5$ layers. The first layer corresponds to the hatched "Mn_2O_5" pyramids, the second to the spotted ones. The angle between the two unit cells is 90°. Several orientations of two layers with respect to one another could thus be drawn.

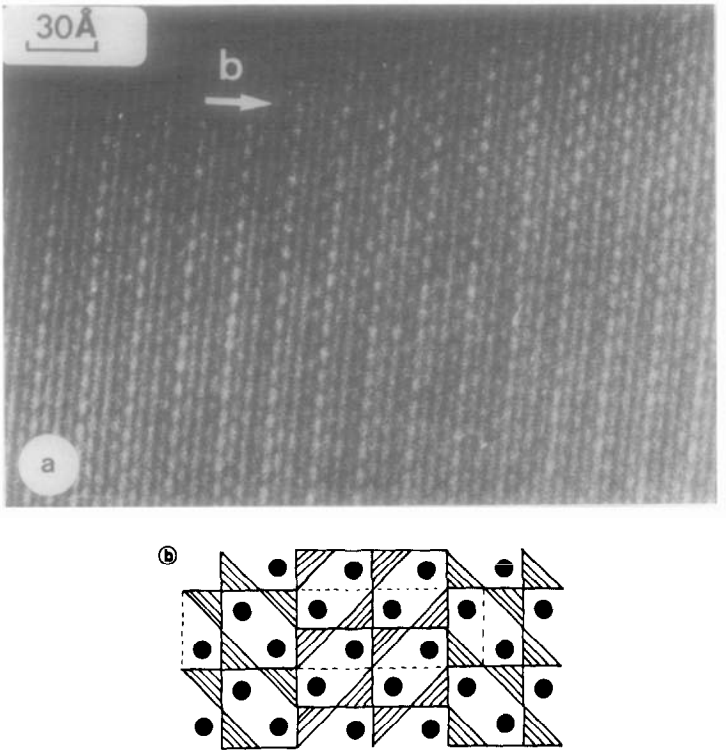

FIG. 8. Micrograph of a crystal showing regular fringes spaced 21.4 Å $\simeq 4a_p\sqrt{2}$. (b) Idealized model (5) for $Ca_2Mn_2O_5$ with $a \simeq a_p\sqrt{2}$ and $b \simeq 4a_p\sqrt{2}$.

the boundaries between the domains may wander as shown in Fig. 7a. It cannot be established whether the pseudocubic domains correspond to stoichiometric $SrMnO_3$ or to the composition $Sr_2Mn_2O_5$ or to intermediate compositions. However, taking into account the fact that the ordering of the oxygen vacancies can take place simultaneously in several directions (Figs. 3, 4) and that the global composition which was found by chemical analysis corresponds to $Sr_2Mn_2O_5$, suggests that the perovskite domains could also be built up of MnO_5 pyramids arranged in an aleatory manner, according to the composition $Sr_2Mn_2O_5$. For instance, the structure could be built up from a disordered stacking of $Sr_2Mn_2O_5$ layers along c, since two successive layers can be translated along different directions with respect one to the other as shown, for example, in Fig. 7b.

Other Ordered Domains

Several crystals exhibit, besides the $Sr_2Mn_2O_5$-type or cubic perovskite domains, ordered domains characterized by different superstructure cells. Such an example is shown on Fig. 8a; one observes a part of a crystal characterized by regular fringes spaced 21.4 Å. This domain can easily be interpreted in terms of an other form of $Sr_2Mn_2O_5$ whose superstructure cell is characterized by the following parameters: $a \simeq a_P\sqrt{2}$, $b \simeq 4a_P\sqrt{2}$, and $c \simeq a_P$. The structure of this form previously proposed for $Ca_2Mn_2O_5$ (5), shows that the composition of the crystal may remain unchanged, whereas the MnO_5 pyramids are connected

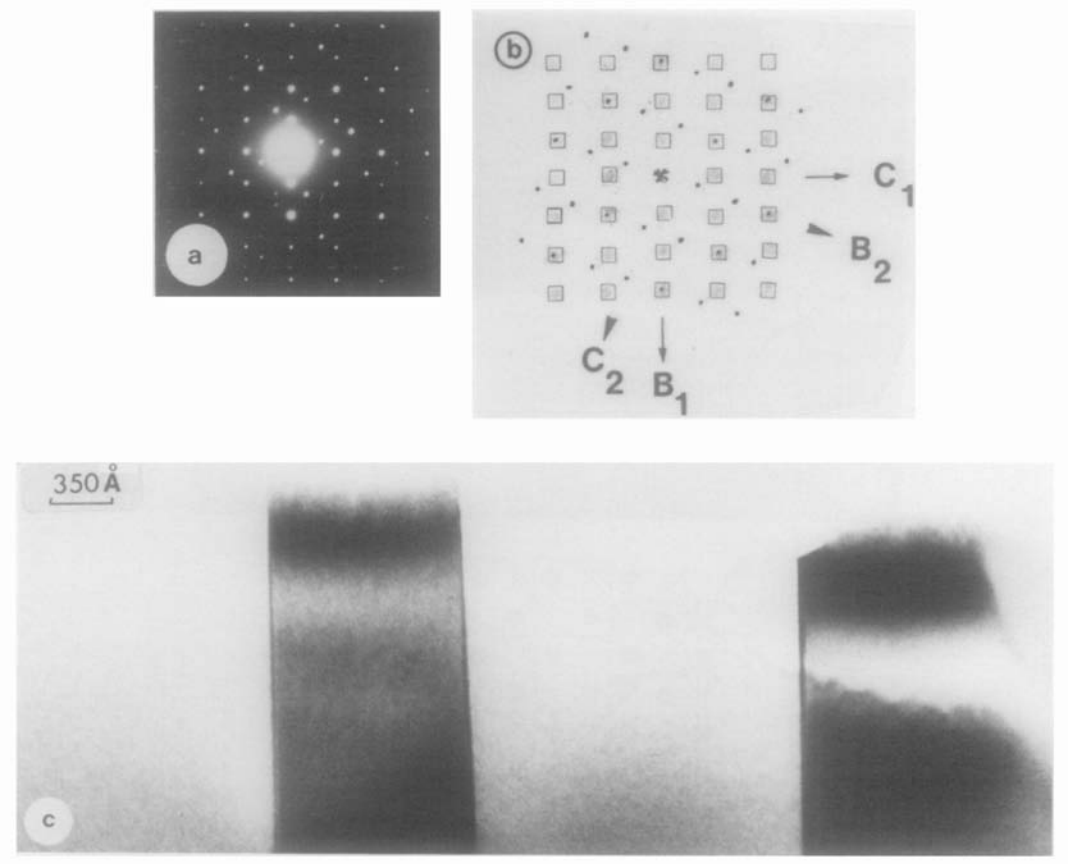

FIG. 9. Observed (a) and schematic (b) electron diffraction patterns of a twined crystal. The twine plane correspond to $(111)_p$ of the ideal cubic perovskite subcell. (c) Low-resolution image of the twined domains.

through their corners in a different manner (Fig. 8b).

Stacking Faults

The electron diffraction patterns of (100) show that some crystals are twined (Fig. 9a) as explained from the schematic drawing of the different zones (Fig. 9b). The corresponding low-resolution image (Fig. 9c) shows domains of various thicknesses ranging from 10 to 150 nm, and characterized by a twine plane parallel to $(111)_P$ with respect to the perovskite subcell. This type of defect can be interpreted as a stacking fault of the SrO_{3-x} layers, corresponding to the sequence |...ccccc h ccccc ...| as shown in Fig. 10. This interpretation is in agreement with the existence of the hexagonal perovskites $SrMnO_3$ (*6*, *11*, *12*), whose

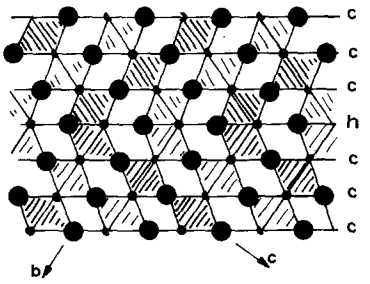

FIG. 10. Idealized drawing of a stacking fault of the SrO_{3-x} layers (large black circles are strontium atoms; small black circles, oxygens; and half circles correspond to ($\frac{1}{2}$O, $\frac{1}{2}\square$) files of the MnO_5 pyramids).

SrO_3-layer stacking involves face-sharing MnO_6 octahedra. In the case of our crystals it cannot be decided whether these faults correspond to a local variation of oxygen content corresponding to the formation of SrO_3 layers or to a simple translation of ordered oxygen-defect $SrO_{2.5}$ layers.

References

1. N. NGUYEN, L. ER-RAKHO, C. MICHEL, J. CHOISNET, AND B. RAVEAU, *Mater. Res. Bull.* **15,** 891 (1980).
2. A RELLER, D. A. JEFFERSON, J. M. THOMAS, R. A. BEYERLEIN, AND K. R. POEPPELMEIER, *J. Chem. Soc., Chem. Commun.,* 1378 (1982).
3. A. RELLER, D. A. JEFFERSON, J. M. THOMAS, AND M. K. UPPAL, *J. Phys. Chem.* **87,** 913 (1983).
4. C. N. R. RAO, J. GOPALAKRISHNAN, AND K. VIDYASAGAR, *Indian J. Chem. Sect. A* **23,** 265 (1984).
5. A. RELLER, J. M. THOMAS, F. R. S., D. A. JEFFERSON, AND M. K. UPPAL *Proc. R. Soc. London Ser. A* **394,** 223 (1984).
6. K. R. POEPPELMEIER, M. E. LEONOWICZ, AND J. M. LONGO, *J. Solid State Chem.* **44,** 89 (1982).
7. K. R. POEPPELMEIER, M. E. LEONOWICZ, J. C. SCANLON, AND J. M. LONGO, *J. Solid State Chem.* **45,** 71 (1982).
8. M. MIZUTANI, V. OKUMA, A. KITAZAWA, AND M. KATO, *J. Chem. Soc. Japan, Ind. Chem. Soc.* **73,** 1103 (1970).
9. T. NEGAS AND R S. ROTH, *J. Solid State Chem.* **1,** 409 (1970).
10. V. CAIGNAERT, N. NGUYEN, M. HERVIEU, AND B. RAVEAU, *Mat. Res. Bull.* **20,** 479 (1985).
11. K. KURODA, N. ISHIZAWA, M. MIZUTANI, AND M. KATO, *J. Solid State Chem.* **38,** 297 (1981).
12. Y. SYONO, S. AKIMOTO, AND K. KOHN, *J. Phys. Soc.* **26,** 993 (1969).
13. A. J. SKARNULIS, E. SUMMERVILLE, AND L. EYRING, *J. Solid State Chem.* **23,** 59 (1978).